THE GEOLOGICAL SOCIETY OF AMERICA®

Evenly spaced columns in the Bishop Tuff (California, USA) as relicts of hydrothermal cooling

Noah Randolph-Flagg, Stephen Breen, Andres Hernandez, Michael Manga, and Stephen Self
Department of Earth and Planetary Science, University of California–Berkeley, Berkeley, California 94720, USA

ABSTRACT

A few square kilometers of the Bishop Tuff in eastern California (USA) have evenly spaced columns that are more resistant to erosion than the surrounding tuff owing to the precipitation of mordenite, a low-temperature (100–130 °C) zeolite. We hypothesize that the columns are a result of instabilities at the liquid water and steam interface as cold water seeped into the still-cooling Bishop Tuff. We use two methods to quantitatively assess this hypothesis. First, scaling shows which hydrodynamic instabilities exist in the system. Second, to account for the effects of multiphase flow, latent heat, and the finite amplitude and temporal evolution of these instabilities we use two-dimensional numerical models of liquid water infiltrating hot tuff. These tests highlight several features of boiling hydrothermal systems. (1) The geometry of at least some convection appears to be broadly captured by linear stability theory that neglects reactive transport, heterogeneity of the host rock, and the finite amplitude of instabilities. (2) Slopes >10% set the wavelength of convection, meaning that these columns formed somewhere with relatively gentle topography. (3) For permeabilities of $>10^{-13}$ m^2, the wavelength of the instability changes through time, slowing infiltration, while for permeabilities $<10^{-15}$ m^2, cooling is dominated by conduction. The spacing and stability of columns increase with higher vertical permeability and decrease with higher horizontal permeability. These columns are a rare window into hydrothermal processes that may be widespread.

INTRODUCTION

Observations of active hydrothermal systems are sparse and, even in geothermal wells, constrained to relatively shallow depths. By contrast, exhumed fossil hydrothermal systems can be fully exposed but preserve the complicated, time-integrated history of each system. In either case, it is difficult to observe the fine-scale dynamic processes transporting heat and mass. Laboratory, analytical, and numerical studies have tried to understand how liquid water and steam interact within permeable rocks and whether they produce periodic instabilities in space (e.g., Woods, 1999; Coumou et al., 2008) and/or time (e.g., Vandemeulebrouck et al., 2005) or produce stable multiphase zones (e.g., Udell, 1985). Hydrothermal alteration in pyroclastic flow deposits, or tuffs, preserves the short-lived cooling history of relatively homogeneous rock and thus offers an unusual opportunity to understand widespread but difficult to observe processes such as groundwater boiling.

The cooling rates of volcanic deposits are accelerated by groundwater flow (e.g., Keating, 2005). Quartz-hosted glass inclusions in the Bishop Tuff (eastern California, USA) suggest that some of the interior of the tuff cooled ~1 °C/yr, consistent with conductive (not advective) cooling models (Wallace et al., 2002). However, evidence of hydrothermal cooling is pervasive in the tuff, including high-temperature fumaroles that persisted for only ~10 yr after the caldera-forming eruption (Holt and Taylor, 1998). The analogous Valley of Ten Thousand Smokes (Alaska) continues to hydrothermally cool a century after the Novarupta eruption (Hogeweg et al., 2005).

Previously reported columnar erosional features in the Bandelier Tuff (New Mexico) are attributed to the interaction between the nonwelded tuff and circulating hot water (Bailey and Self, 2010). We integrate field observations of unstudied columns in the Bishop Tuff, theory, and numerical simulations to evaluate the hypothesis that these columns are relicts of hydrothermal instabilities.

GEOLOGIC SETTING

The Bishop Tuff formed at the eastern foot of the Sierra Nevada range after the 760 ka Long Valley explosive rhyolite (74%–78% SiO_2) eruption (Hildreth and Wilson, 2007). The tuff produced by this 600–650 km^3 supereruption extends >70 km downslope of the Long Valley caldera, and, within the caldera, up to 1.5 km thick. The tuff erupted over a few days to years (Hildreth and Wilson, 2007) with welding, high-temperature vapor phase zones, devitrified fumarolic mounds (e.g., Holt and Taylor, 1998), and elutriated gas-escape pipes all forming soon after due to reactions between volatiles and rhyolitic glass.

OBSERVATIONS

Evenly spaced erosional columns pervade at least a few square kilometers of the nonwelded Bishop Tuff (Fig. 1). The highest elevation outcrops are below the oldest paleolake terrace at ~2250 m elevation (Bailey et al., 1976). Columns occur in some (but not all) nonwelded regions of the tuff; they are not visible in any welded or vapor-phase altered regions. Nearly identical columns exist in white tuff with >10 cm pumice and lithic clasts, some of the first tuff erupted (ignimbrite unit Ig1Ea; Hildreth and Wilson, 2007), and in more homogeneous pinkish tuff with <1 cm clasts (Fig. DR1 in the GSA Data Repository[1]), some of the last tuff erupted (Ig2E; Hildreth and Wilson, 2007).

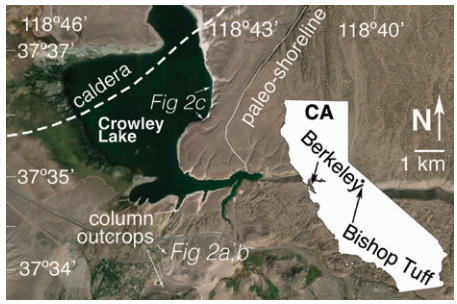

Figure 1. Map of Bishop Tuff near Lake Crowley reservoir (California, USA). White dashed line shows approximate location of the caldera topographic margin from Bailey et al. (1976).

The erosional columns are usually vertical with some tilted (Fig. DR2) and rare branching columns (Fig. 2A, bottom right). A survey of hundreds of columns (Fig. DR3B) suggests regular spacing locally (~0.8–4 m column center to column center) with column diameters ranging from 0.3 to 1 m. Figure 2C is representative of outcrops along the northeast shore of the human-made Lake Crowley, where unaltered tuff has been eroded since A.D. 1941 to expose columned caves. Beach and road outcrops have column nubs that have similar spacing and morphology. A few of these exposures appear to have north-northeast–south-southwest–trending lineaments of columns and rarer parallel and pseudocellular walls with roughly similar spacing (Fig. DR3A). Columns persist with constant aspect

[1]GSA Data Repository item 2017348, additional figures, animations, and an example input file to HYDROTHERM, is available online at http://www.geosociety.org/datarepository/2017/ or on request from editing@geosociety.org.

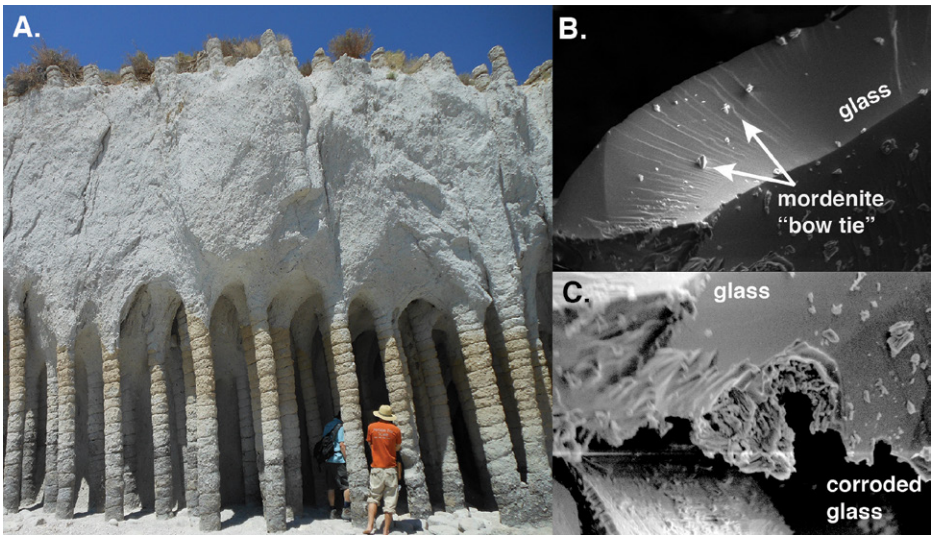

Figure 2. A, B: Scanning electron microscope images for the columns (37°34′20.8″N, 118°42′57.9″W) showing distinctive mordenite crystal structures on pitted volcanic glass fragments. C: Photo from beach of Lake Crowley (California, USA; people for scale). Columns extend from wave eroded caves through tuff and up above the outcrop.

ratio through minor compositional changes in the tuff and are continuous across thin horizontal Plinian deposits. Vertical elutriation pipes are crosscut by tilted columns (Fig. DR2). All columns that we observed have joints perpendicular to the column with a width/joint spacing ratio of ~0.8. This ratio is similar to the ratio of vertical joints to horizontal sedimentary bed thickness. This suggests that similar differences in the elastic properties of horizontal layers that cause strain localization (e.g., Bai et al., 2000) may be occurring on the vertical cylindrical columns during cooling or unloading.

The quarry outcrops (Fig. DR1) show the base of the Bishop Tuff with a thick (>5 m) white Plinian deposit overlain by ~8 m of pinkish tuff with no erosional columns. The columns grow from nothing to ~50 cm diameter over 3 m of massive tuff. Outcrops are mostly within several meters of the Bishop Tuff base and, in some places, hundreds of meters of overlying tuff have been eroded since the columns formed. Similar columns in the Bandelier Tuff also exist a few meters above the base of the tuff (Bailey and Self, 2010).

X-ray diffraction (XRD) spectra show that the only mineralogical difference between the columns and surrounding material is the mineral mordenite [$(Ca, Na_2, K_2)Al_2Si_{10}O_{24}•7H_2O$], a low-temperature zeolite also found in similar columns in the Bandelier Tuff (Bailey and Self, 2010). XRD of the uncemented tuff surrounding the columns shows no measureable zeolite precipitation (Fig. DR4); samples taken from the columns show mordenite precipitation. Scanning electron microscope images from the columns show distinctive 1–3 μm mordenite "bow-tie" crystals every few micrometers on pitted volcanic glass shards (Figs. 2B and 2C). Dry experiments in Yucca Mountain Tuff (Nevada) found mordenite growth when heated to 120–200 °C, although those samples also had clinoptilite [$(Na, K, Ca)_2$-$3Al_3(Al, Si)_2Si_{13}O•12H_2O$], another zeolite. Field observations in the Yucca Mountain Tuff using illite and smectite ratios as a paleothermometer imply that clinoptilolite forms from 90 to 100 °C, mordenite forms from 100 to 130 °C, and analcime forms from 175 to 200 °C (Bish and Aronson, 1993).

HYPOTHESIS

We test the "heat-pipe" steam-liquid counterflow hypothesis. In our conceptual model, the tuff is emplaced and instantly begins to slump along paleodrainages. At the surface, where heat can be transported by wind (forced convection), the tuff cools quickly. By contrast, the interior of the tuff cools much more slowly due to conduction alone. Water pools in low-lying regions, forming ponds or lakes, and then percolates into the tuff. Infiltrating water heats and boils, generating evenly spaced fingers of upwelling steam that condenses before reaching the surface, and downwelling water that boils at its base (Bailey and Self, 2010). We suggest that downwellings may precipitate mordenite because ions are only transported in the liquid phase and, in plan view, the columns are small relative to the surrounding material, implying that they record the denser phase. Later, when the tuff begins to erode (Fig. 3), these mordenite-cemented downwellings are preserved while the uncemented tuff is eroded away.

Although columnar jointing is common in the welded Bishop Tuff, jointing cannot explain the large distances between columns, the lack of visible fractures in the surrounding material, or the hydrothermal alteration. These columns crosscut subvertical elutriation pipes and are cemented by a low-temperature zeolite, indicating that they formed after the elutriation pipes and at lower temperatures. Similarly, fossil fumaroles caused by the escape of water and gas trapped beneath or within pyroclastic density current deposits produce high-temperature (>500 °C) alteration and devitrification (e.g., Holt and Taylor, 1998) rather than the low-temperature alteration we observe.

SCALING

If surface water sank into the cooling tuff from above, there would be three possible drivers of groundwater flow: thermal convection within the steam or liquid, instabilities at the steam-liquid interface, and topographically forced flow.

Thermal convection is the process by which cold dense material sinks and warm buoyant material rises. Porous media thermal convection occurs if the Rayleigh-Darcy number is greater than the critical Rayleigh number, i.e., $Ra > Ra_{CR} = 4\pi^2$ (see Phillips, 1991). Using reasonable values (Table DR1) we find that the relatively dense liquid water convects while the steam does not (Fig. DR5). The velocity of this convection in the liquid phase is given by Darcy's law:

$$\boldsymbol{u}_{\text{conv}} = \frac{k}{\mu_l}\nabla P = \frac{k}{\mu_l}\rho_l g \alpha_l \Delta T, \qquad (1)$$

where k is the permeability, μ is the viscosity, ρ is the density, and the pressure gradient ∇P is given by buoyancy, where g is the acceleration of gravity, α is the thermal expansivity for a

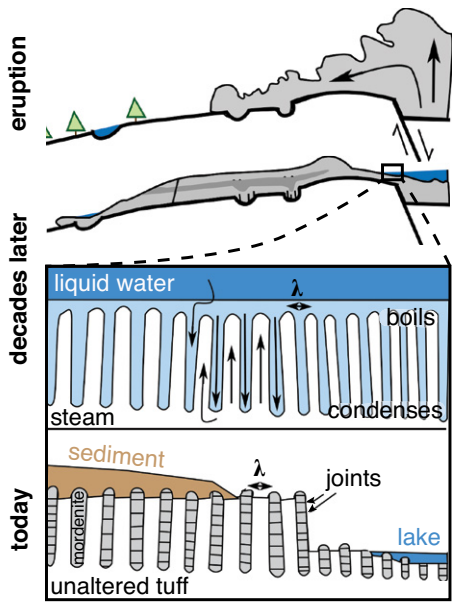

Figure 3. Schematic illustration of the Long Valley caldera (California, USA) forming eruption (top), our hypothesis of the still-cooling deposit (middle), and the modern outcrop similar to that in Figure 2C (bottom). λ denotes the spacing of columns and downwellings.

change in temperature, ΔT, and the subscript l denotes the liquid phase.

If we assume that liquid water seeps into the tuff due to its own weight, the Darcy velocity of the interface ($\boldsymbol{u}_i$) is

$$\boldsymbol{u}_i = (1-F)\boldsymbol{u}_l = (1-F)\frac{k}{\mu_l}\nabla P = (1-F)\frac{k}{\mu_l}\rho_l g, \quad (2)$$

where F is the fraction that vaporizes due to boiling and $\boldsymbol{u}_l$ is the Darcy velocity of the liquid phase. Comparing Equations 2 and 3, this Darcy interfacial velocity dominates if $(1 - F) > \alpha\Delta T$, where F is the mass fraction vaporizing given by

$$F = (1 + S\phi)^{-1} = [1 + \phi L/(c_p \Delta T)]^{-1}, \quad (3)$$

where ϕ is the porosity and S is the saturation, which is equal to the latent heat of vaporization L divided by the heat capacity c_p, and the temperature change between the superheated steam and the boiling water, ΔT (Woods, 1999). For representative values, the mass fraction vaporizing should be ~0.7 and the interfacial velocity will be ~0.3 $\boldsymbol{u}_l$ or ~100 $\boldsymbol{u}_{conv}$. Therefore, the processes occurring at the liquid water-steam interface dominate thermal convection.

Short-wavelength perturbations to a planar liquid front seeping into steam are damped by thermal diffusion, while long-wavelength downwellings are suppressed by an increase in vapor pressure (Woods, 1999). Linear stability analysis (Sondergeld and Turcotte, 1978; Woods, 1999) predicts that the spacing between gravitational fingers at the onset of the instability is meters, similar to observations (Fig. 3).

Although we do not know the topography of the tuff immediately after the eruption, for the columns to form the interfacial Darcy velocity must have been greater than the Darcy velocity due to topographic flow (u_{topo}). That is,

$$\boldsymbol{u}_i > \boldsymbol{u}_{topo} = (1-F)\frac{k}{\mu_l}\rho_l g > \frac{k}{\mu_l}\rho_l g G = (1-F) > G, \quad (4)$$

where G is the topographic grade. This implies that a grade of 10%–100% would be required to dominate the flow (see Phillips, 1991). An average stream gradient for the modern Owens River is <0.01%, so the columns could have formed beneath either a lake or stream. Assuming a high permeability ($k = 10^{-13}$ m^2) and no boiling (F = 0), the fastest infiltration rate is ~1 m/yr. The modern average rainfall near Long Valley is ~0.5 m/yr. Integrating the precipitation over a catchment, this implies that a reservoir could maintain a constant water level even with rapid infiltration.

Scaling arguments and stability analysis suggest that the liquid water–steam interface is the source of the columnar geometry of flow, that this interface is unstable at the meter length scale, and that there is enough water in the region to sustain a roughly continuous hydrothermal system and provide upper and lower bounds on the rate that the tuff cooled. However, these scalings assume a sharp liquid water–steam interface without multiphase flow. The linear stability analysis also identifies the wavelength of the initial instability but does not capture the finite amplitude and temporal evolution of instabilities such as boiling along the sides of downwellings. These limitations motivated our two-dimensional numerical simulations.

NUMERICAL MODEL

To test our hypothesis, we use the U.S. Geological Survey program HYDROTHERM (Kipp et al., 2008) to solve the coupled multiphase groundwater and energy conservation equations in two dimensions. These models fully account for the effects of latent heat and two-phase flow but do not capture chemical reactions. Our two objectives are (1) to see if numerical models using known rock properties produce the spacing, formation temperatures, and shape of the observed columns, and (2) to systematically change permeability and topography to identify the patterns of flow that develop when a tuff is cooled by water from above.

We impose closed (no fluid or heat flow) boundaries at the base and sides and a fixed-temperature, fixed-pressure boundary (30 °C, 20 atm) at the surface. Many of the column outcrops (e.g., Fig. 2C) are exposed due to ~200 m of erosion of overlying tuff. The upper boundary condition reflects these estimates of erosion below a shallow lake of relatively constant head while hydrostatic pressure is assumed in the rest of the model. Because steam is highly compressible, the pressure within the tuff relates to its cooling history and may change some details of flow geometry. We assume an initial tuff temperature of 500 °C with temperatures grading in the upper 2 m to 30 °C and a slight perturbation of the isotherms at the center of the domain. This upper boundary temperature does not appear to set the wavelength of convection but is necessary for numerically stability in the first several time steps. Unless otherwise stated, all models use Corey relative permeability functions.

RESULTS

Geometry of Flow

At low permeabilities, <10^{-15} m^2, liquid water infiltrates the tuff with a narrow, <1 m multiphase boiling zone. Temperature, pressure, and phase do not vary laterally. For slightly higher permeabilities (10^{-14} m^2), the cooling path is the same until periodic undulations begin at ~12 m depth. These undulations form at the boundaries of a thickening, isothermal, two-phase zone. Within this two-phase zone, periodic fingers of saturation (0.1–1) correspond to undulations in the two phase–single phase interfaces. Fingers remain at a constant ~3 m spacing until the first finger reaches the bottom boundary. Upon reaching this lower boundary, water condenses and flows along the base. At higher permeability (>10^{-13} m^2), unsteady fingers form immediately in the two-phase zone. These fingers coalesce into a single downwelling, which sweeps across the domain. Unlike the lower permeability simulations, the downwelling fingers remain largely steam dominated (0.3 saturation) until they reach the base of domain (Fig. 4).

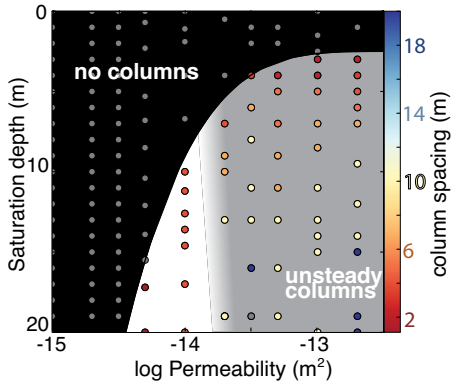

Figure 4. Regime diagram for simulations. Each vertical line of points shows a single simulation that progresses from 0 to 20 m in saturation depth. Gray circles show no columns. Colors show column spacing in meters. White background shows range with persistent columns, gray background shows unsteady columns, and black shows no columns.

Topography greater than the liquid water thickness at the onset of fingering appears to set the wavelength of fingering; i.e., one large swale creates two large downwellings and a single large upwelling (e.g., Fig. DR9). Relative permeability functions that produce sharper saturation gradients have more stable fingers. The geometry of flow does not appear to be sensitive to changes in initial temperature between 200 and 800 °C, although these changes do affect the rate of cooling. Finally, higher vertical permeability seems to increase the stability of fingers while higher horizontal permeability increases the unstable cannibalization of fingers (Fig. DR10).

Rate of Cooling

At low permeabilities, <10^{-15} m^2, cooling follows the conductive cooling path, requiring ~40 yr to cool 20 m of tuff (assuming a thermal diffusivity of 10^{-6} m^2/s). At higher permeabilities, 10^{-14} m^2, liquid water infiltrates the tuff at the rate of conductive cooling until fingering begins. Once fingering begins, the tuff cools at the rate of advective cooling to 100 °C. At even higher permeabilities, 10^{-13} m^2, fingering begins immediately with many small downwellings. However, as the fingers coalesce they advance at a slower rate than the advective cooling rate, cooling 20 m of tuff to ~100 °C in only 4 yr (Fig. 5).

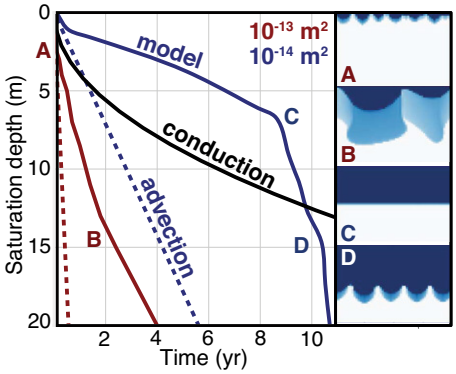

Figure 5. Black line shows tuff cooling by conduction. Red is 10^{-14} m^2 permeability and blue is 10^{-13} m^2 permeability. Dotted lines show advective cooling assuming no vaporization. Solid lines show numerical model results. Boxes show 20 × 20 m simulations where dark blue is liquid water saturated and white is steam saturated.

DISCUSSION AND CONCLUSIONS

Low-temperature hydrothermal alteration in the Bishop Tuff cements evenly spaced columns. This alteration pervades at least a few square kilometers of Bishop Tuff and appears to form in very different lithofacies with different hydrologic properties (e.g., units Ig1Ea and Ig2E). We show that liquid water infiltrating tuff from above can produce evenly spaced gravitational fingers. Scaling shows that the liquid water–steam interface probably is the source of the instability that generates columnar flow. At high permeabilities, numerous downwellings quickly coalesce into a large downwelling, which migrates laterally across the domain. Only for intermediate permeabilities are numerous downwellings stable in time and space. These stable downwellings advance into the tuff at the rate of fluid advection. The spacing of these columns in simulations is, in order of magnitude, similar to the spacing we observe in the field and similar to linear stability analysis (Woods, 1999). The intermediate permeability simulations may be stabilized due to saturation gradients between upwelling and downwelling fluid (e.g., Coumou et al., 2008).

Our two-dimensional flow simulations roughly capture the spacing of the observed columns. Although we do not explicitly model mineral precipitation, changes in effective permeability for different phases are captured by relative permeability functions. Mordenite crystals are small relative to pore size (Figs. 2A and 2B), and in X-ray computed microtomography scans are not large enough to be seen or to change the pore network (Fig. DR11). The high porosity of the tuff and fibrous mineral structure of mordenite imply that precipitation and dissolution may have relatively small effects on permeability and large effects on strength. Future laboratory experiments may contribute a new understanding to the kinetics of mordenite precipitation and the mechanical consequences of these reactions. Although dominantly columns, mordenite alteration in the Bishop Tuff is diverse (Fig. DR3A), including rolls, hexagonal cells, and tilted columns all with meter-scale spacing and patterns analogous to those in three-dimensional Rayleigh-Bénard convection. Extension of our model to reactive three-dimensional flow may offer new insights into the rates and patterns of hydrothermal flow.

If our hypothesis is correct, the Bishop Tuff columns are a rare window into the geometry and rates of flow in many geothermal systems, fumarolic areas, and caldera lakes. This model also implies that water pooled in and near the Long Valley caldera soon after its eruption.

ACKNOWLEDGMENTS

We are grateful to S. Barker, J. Vandemeulebrouck, and two anonymous reviewers for helpful reviews, and to W. Hildreth, T. Driesner, and S. Ingebritsen for helpful comments on the manuscript. Randolph-Flagg was supported by the National Science Foundation Graduate Research Fellowship (DGE 1106400), while other authors were supported by the National Science Foundation (NSF-1521855) and the University of California Berkeley Larsen grant. X-ray microtomography was enabled by access to the Lawrence Berkeley National Lab Advanced light source on beamline 8.3.2. We thank Dula Parkinson for guidance with μXRT imaging and image processing.

REFERENCES CITED

Bai, T., Pollard, D.D., and Gao, H., 2000, Explanation for fracture spacing in layered materials: Nature, v. 403, p. 753–756, https://doi.org/10.1038/35001550.

Bailey, J.E., and Self, S., 2010, The properties and formation of erosional pipe-shaped structures in ignimbrites around the Valles Caldera: Geological Society of America Abstracts with Programs, v. 42, no. 5, p. 51.

Bailey, R.A., Dalrymple, G.B., and Lanphere, M.A., 1976, Volcanism, structure, and geochronology of Long Valley Caldera, Mono County, California: Journal of Geophysical Research, v. 81, p. 725–744, https://doi.org/10.1029/JB081i005p00725.

Bish, D.L., and Aronson, J.L., 1993, Paleogeothermal and paleohydrologic conditions in silicic tuff from Yucca Mountain, Nevada: Clays and Clay Minerals, v. 41, p. 148–161, https://doi.org/10.1346/CCMN.1993.0410204.

Coumou, D., Driesner, T., and Heinrich, C.A., 2008, Heat transport at boiling, near-critical conditions: Geofluids, v. 8, p. 208–215, https://doi.org/10.1111/j.1468-8123.2008.00218.x.

Hildreth, W., and Wilson, C.J., 2007, Compositional zoning of the Bishop Tuff: Journal of Petrology, v. 48, p. 951–999, https://doi.org/10.1093/petrology/egm007.

Hogeweg, N., Keith, T.E.C., Colvard, E.M., and Ingebritsen, S.E., 2005, Ongoing hydrothermal heat loss from the 1912 ash-flow sheet, Valley of Ten Thousand Smokes, Alaska: Journal of Volcanology and Geothermal Research, v. 143, p. 279–291, https://doi.org/10.1016/j.jvolgeores.2004.12.003.

Holt, E.W., and Taylor, H.P., 1998, $^{18}O/^{16}O$ mapping and hydrogeology of a short-lived (≈ 10 years) fumarolic (> 500° C) meteoric-hydrothermal event in the upper part of the 0.76 Ma Bishop Tuff outflow sheet, California: Journal of Volcanology and Geothermal Research, v. 83, p. 115–139, https://doi.org/10.1016/S0377-0273(98)00014-6.

Keating, G.N., 2005, The role of water in cooling ignimbrites: Journal of Volcanology and Geothermal Research, v. 142, p. 145–171, https://doi.org/10.1016/j.jvolgeores.2004.10.019.

Kipp, K.L., Jr., Hsieh, P.A., and Charlton, S.R., 2008, Guide to the revised ground-water flow and heat transport simulator: HYDROTHERM—Version 3: U.S. Geological Survey Techniques and Methods 6-A25, 160 p.

Phillips, O.M., 1991, Flow and Reactions in Permeable Rocks: Cambridge, UK, Cambridge University Press, 296 p.

Sondergeld, C.H., and Turcotte, D.L., 1978, Flow visualization studies of two-phase thermal convection in a porous layer: Pure and Applied Geophysics, v. 117, p. 321–330, https://doi.org/10.1007/BF00879757.

Udell, K.S., 1985, Heat transfer in porous media considering phase change and capillarity—The heat pipe effect: International Journal of Heat and Mass Transfer, v. 28, p. 485–495, https://doi.org/10.1016/0017-9310(85)90082-1.

Vandemeulebrouck, J., Stemmelen, D., Hurst, T., and Grangeon, J., 2005, Analogue modeling of instabilities in crater lake hydrothermal systems: Journal of Geophysical Research, v. 110, B02212, https://doi.org/10.1029/2003JB002794.

Wallace, P.J., Dufek, J., Anderson, A.T., and Zhang, Y., 2002, Cooling rates of Plinian-fall and pyroclastic-flow deposits in the Bishop Tuff: Inferences from water speciation in quartz-hosted glass inclusions: Bulletin of Volcanology, v. 65, p. 105–123, https://doi.org/10.1007/s00445-002-0247-9.

Woods, A.W., 1999, Liquid and vapor flow in superheated rock: Annual Review of Fluid Mechanics, v. 31, p. 171–199, https://doi.org/10.1146/annurev.fluid.31.1.171.

Manuscript received 20 April 2017
Revised manuscript received 1 August 2017
Manuscript accepted 2 August 2017

Printed in USA